# Spreading of dynamically crosslinked polydimethylsiloxane drops

Kyujin Ko[1], Krishnaroop Chaudhuri[1], Junyong Park[2], Sanghyuk Wooh[2], Benjamin M Yavitt[1,3], and Jonathan T Pham[1,3,*]

[1]Department of Chemical and Environmental Engineering, University of Cincinnati, Cincinnati, OH, 45221, USA.

[2]Department of Chemical Engineering, Chung-Ang University, 84 Heukseok-ro, Dongjak-gu, Seoul, 06974, Republic of Korea.

[3]Department of Mechanical and Materials Engineering, University of Cincinnati, Cincinnati, OH, 45221, USA.

Email: Jonathan.Pham@uc.edu

# Abstract

Dynamically crosslinked polymer networks, characterized by non-permanent bonds, offer unique viscoelastic properties that can be used for various applications such as self-healing coatings and reusable adhesives. This study investigates the spreading behavior of a silicone polymer network with dynamic imine bonds, focusing on the relationship between material properties and spreading dynamics. We prepare polydimethylsiloxane (PDMS) networks with varied rheological properties by adjusting the ratio of amine and aldehyde groups and curing conditions. The spreading of PDMS spherical drops is investigated on surfaces with different surface energies, with the process quantified by measuring the contact length and height over time. Our findings reveal that higher modulus spheres spread more slowly, and that the spreading length increases more on high energy surfaces. This research could provide insights for developing coatings and adhesives with tunable properties by studying the interaction between transiently-crosslinked polymers and substrates during spreading.

## Introduction

Dynamically crosslinked polymer networks are linked together by non-permanent, reversible bonds, such that the polymer chains can rearrange relatively easily[1-4]. These materials have unique viscoelastic properties that are governed by the concentration and the kinetics of the dynamic bonds acting as crosslinks[5-7]. Such materials can be applied as self-healing protective coatings[8-11], reuseable adhesives[12-15], and wearable sensors[16-18], among others[19-21]. Recent studies have demonstrated that the modulus of dynamically crosslinked polymers can be precisely controlled by adjusting the amount of crosslinker in the network[22-24], allowing for fine-tuning the mechanical properties of dynamic networks. Moreover, these materials are often put onto various substrates by spray-coating[8, 25-26], 3D printing[25, 27-30], and spin-coating[31-33] for the desired end-use application. Given that coating and printing processes begin with spreading of the materials on the substrate, it is important to understand how these dynamic networks spread on the surface.

Dynamically crosslinked polymers are frequently used in coatings and adhesives to control wetting and spreading behavior[15, 32, 34-38]; however, most studies primarily focus on material formulations and adhesive strength, with limited exploration of the spreading behavior of the material itself. In this context, previous research has explored the spreading of viscoelastic drops, such as polymer melts and dilute polymer solutions. Some of the most relevant efforts are from the 1960s, which investigated how polymer melts with different viscosities spread on substrates with varying surface energies[39-41]. These studies demonstrate that the radial growth of the melt drop scales with the surface energy, viscosity, and some characteristic length, allowing for a master curve to be developed. Similarly, studies on polymer solutions with different viscosities have shown that the maximum drop radius decreases with increasing solution concentration and viscosity[42-43]. From the surface energy perspective, high surface energy substrates enhance wettability, leading to better spreading of viscoelastic polymer droplets, while low surface energy substrates can result in poor wetting and coatability[44-45]. The balance of surface energy and rheological properties can also affect the geometric profile of spreading drops, sometimes leading to a protruding foot at the contact line[39, 41, 46-47]. While preceding studies have investigated how rheological properties and surface energy relates to spreading, these have focused primarily on traditional polymer melts and solutions.

In this manuscript, we investigate the spreading of a spherical drop comprising a polydimethylsiloxane network, crosslinked with reversible covalent imine bonds (imPDMS). These are prepared by mixing an aldehyde functionalized crosslinker with PDMS chains having amine groups along the backbone. The aldehyde reacts with the amine to create an imine bond, which will revert back into the aldehyde and amine. imPDMS drops are placed onto a surface to study spreading. Variables to be considered include the aldehyde to amine ratio, the curing time, and the surface energy of the substrate. We quantify spreading by measuring the contact length ($L$) and height ($H$) over time (Figure 1). Materials with higher crosslinker ratios and longer curing times tend to spread slower than lower crosslinking ratios and shorter curing times. imPDMS drops spread less on lower surface energy surfaces, although the effect of surface energy is less dominant than the effect of crosslinking ratio and curing time. This

suggests that the rheological properties are more dominant than the surface energy in spreading dynamics of imPDMS drops.

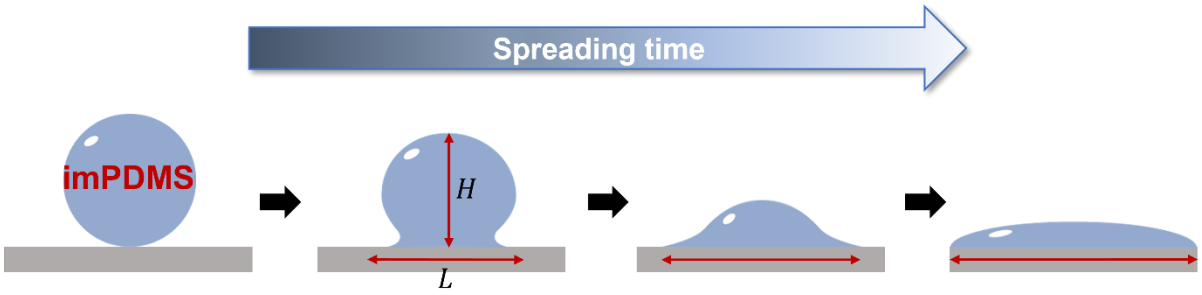


Figure 1. Schematic diagram of spreading process, showing different spreading profiles. The drop starts in a spherical shape, and can be followed by a bell shape, fried egg shape, and spherical cap shape (from left to right). The height ($H$) and contact length ($L$) are measured.

**Results and discussion**

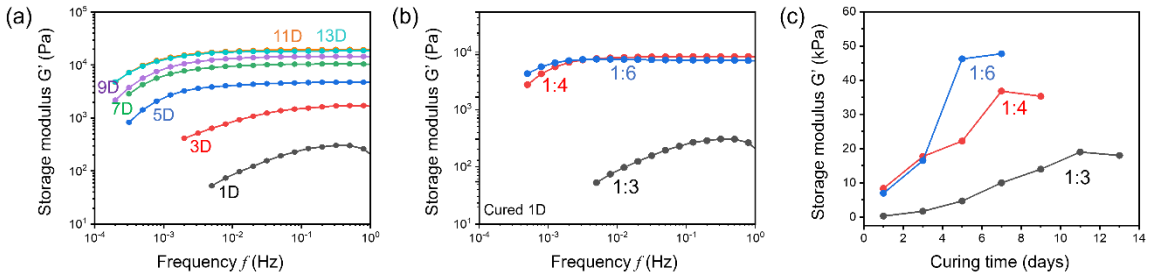


Figure 2. Rheology of imPDMS (a) 1:3 mixing ratio for different curing times and (b) various mixing ratios after curing for 1 day, (c) Change in plateau storage modulus by increasing curing time, for different mixing ratios.

*Materials characterization*. The imPDMS materials are prepared by mixing a dialdehyde with amine-functionalized PDMS at different molar crosslinking ratios (1:3, 1:4, and 1:6) followed by curing at 65°C in an oven for a predefined number of days. Both the curing time and molar ratio are used to control the mechanical properties, which is characterized by oscillatory shear rheology. The amount of curing time in the oven plays a significant role in the mechanical properties. Taking the 1:3 ratio as an example, increasing the curing time from 1 day to 13 days results in a gradual increase of the storage modulus ($G'$); the storage modulus approaches a plateau as a function of curing days after ~11 days (Figure 2a) (see Fig. S1 for 1:4 and 1:6 ratios and crossover frequency). The plateau region extends to lower and lower oscillatory frequency, suggesting an increase in the terminal relaxation time with increasing plateau modulus (see Fig. S1 for crossover). The stiffening may be the result of increased crosslinking due to decreased humidity or due to chains reaching more preferred configurations with longer times in the oven at elevated temperature[48]. Amine groups react with the dialdehydes to form imine bonds, releasing water molecules during crosslinking[49]. The gradual evaporation of water molecules from the reaction while curing at 65°C would limit hydrolysis, resulting in stiffer

materials. On the other hand, in high humidity conditions, equilibrium shifts towards amines and aldehydes. Nevertheless, this effectively makes curing time a processing parameter. The modulus can also be adjusted by the molar ratio, which controls the imine crosslinker concentration. For example, at a constant curing time of 1 day, increasing the molar ratio from 1:3 to1:4 to 1:6 leads to an increase in the crosslinking density and the storage modulus $G'$ (Figure 2b). The storage modulus with respect to curing time and mixing ratio ranges from ~0.3 to 48 kPa by adjusting the mixing ratio from 1:3 to 1:6 and curing time from 1 day to 14 days (Figure 2c). Hence, both the curing time and the ratio of crosslinker will be considered. These qualitative rheological characteristics will aid in understanding how imPDMS drops spread on a substrate.

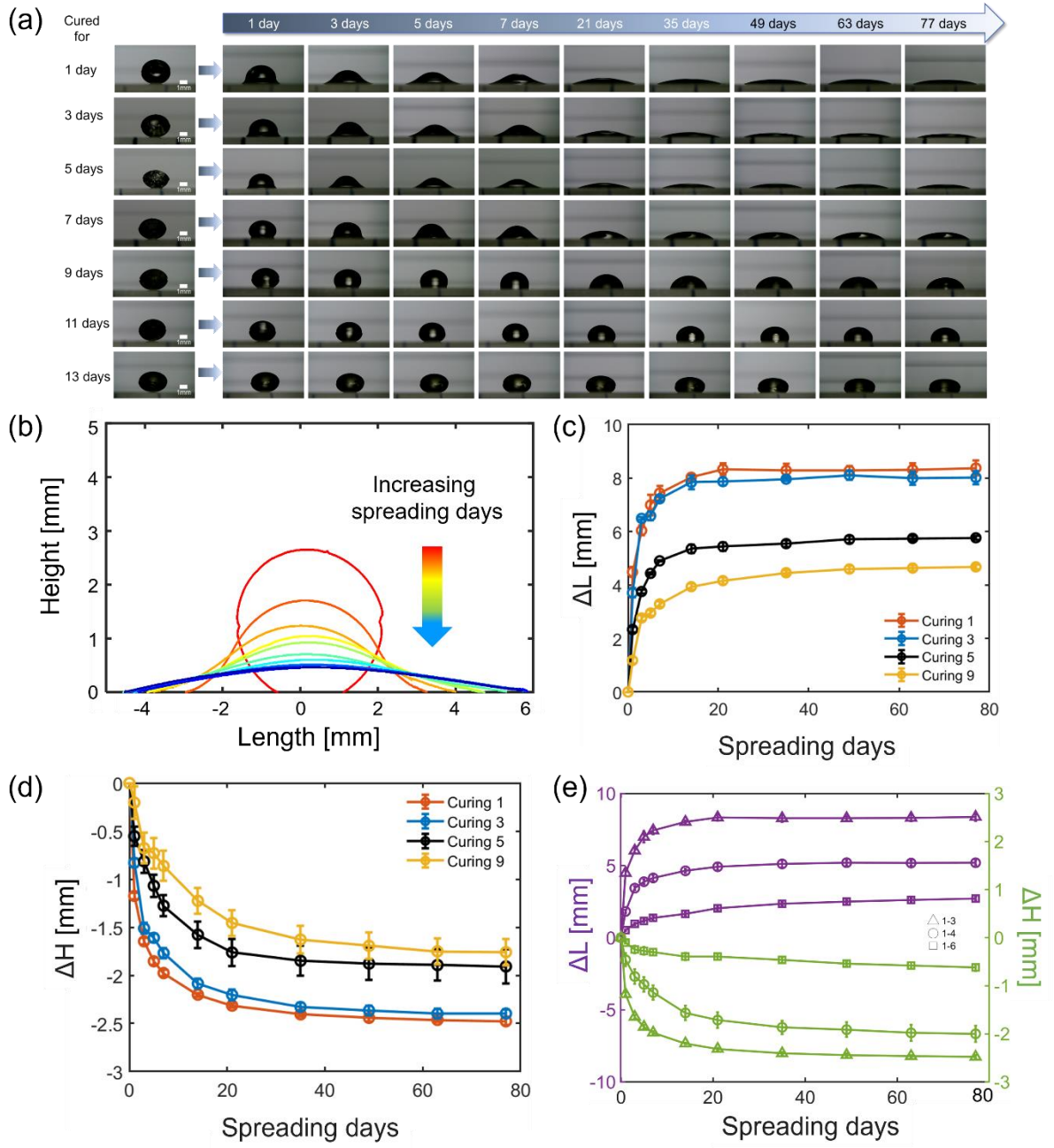

Figure 3. (a) Time dependent spreading of imPDMS of 1:3 ratio on glass based on various curing time, (b) Spreading profile, (c) length change ($\Delta L$), (d) height change ($\Delta H$) of 1:3 ratio, and (e) $\Delta L$ and $\Delta H$ for different mixing ratio at curing 1 day on glass

*Spreading on glass*. The spreading of imPDMS drops on a clean glass substrate is investigated for 77 days, revealing clearly different extents of spreading and shape profiles, depending on both the curing time and the crosslinking ratio. Here we consider the 1:3 ratio as our example case (Figure 3a). Driven by surface energy, the imPDMS spreads along the substrate. In general, the increase in contact area between the imPDMS and substrate dominates over the variation in height. In the early spreading stage, a "bell shaped" geometry (e.g. Figure 1) with small footprint is observed, which is particlarly clear for lower curing days (1 day to 7 days). Subsequently, a "fried egg-like" shape (e.g. Figure 1) is observed as the height slowly decreases due to the relaxation of the polymer network, facilitated by the reconfiguration of the dynamic, reversible imine linkages. When sufficient changes in length and height have passed after longer times (e.g. ~21 days), it exhibits a spherical cap shape (e.g. Figure 1). It should be noted that imPDMS spreading experiments are conducted at ambient humidity. Over the long spreading times, the material likely absorbs water molecules, which can influence imine bond stability[50]. Imine bonds can be hydrolyzed to amine and aldehyde groups by water molecules, resulting in more liquid-like properties. However, it is challenging to decouple the effects of humidity and the bond exchange rate on the viscoelastic response. For a longer curing times of 9 or 11 days, no bell or fried egg geometry is observed during the spreading process, and for 13 days, there is almost no change to the shape. This suggests that the effect of ambient humidity is a relatively slow when the material is already highly crosslinked and that the dynamic bond exchange rate dictates the viscoelastic relaxation. In general, the 1:4 and 1:6 ratio imPDMS show similar behavior, but shifted to slower spreading due to the increase in modulus and the relaxation time (Fig. S1); the images are provided in the supporting information (Figs. S2 and S3).

To gain a better picture of the spreading dynamics, the 2D profiles for a 1:3 imPDMS are stacked on a single coordinate system as a function of spreading days (Fig. 3b). Initially, the spherical imPDMS rapidly spreads along the substrate and then forms a bell shape with a foot. The height gradually decreases due to network relaxation as the shape shifts from multiple curvature signs (e.g. after spreading for 1 day) to a single curvature (e.g. after spreading for 35 days). Eventually, the contact length elongates while the height diminishes, reaching a stable spherical cap geometry. We quantified the length change ($\Delta L$) (Fig. 3c), defined as the length at a given spreading day minus the initial length at 0 spreading days ($L_0$). $\Delta L$ exhibits an exponential-like growth initially and then plateaus. This illustrates that the drop stops spreading after sufficient time has passed. Drops reach the plateau region more quickly for lower curing times and lower mixing ratios due to lower crosslinking (and faster relaxation). In contrast, the change in height ($\Delta H$) (Fig. 3d), defined as the height at a given spreading day minus the initial height at 0 spreading days ($H_0$), demonstrates an exponential-like decay before reaching a plateau. $\Delta L$ reaches the plateau state more rapidly than $\Delta H$. For example, consider the 1:3 drops after 1 day of curing: $\Delta L$ reaches a plateau after ~20 days, while $\Delta H$ approaches a steady state

but continues to decrease throughout the 77 days. In general, similar behaviors are observed for the other crosslinking ratios (1:4 and 1:6), albeit with different quantitative values due to the increases in modulus and relaxation time. (See SI Figs. S2 and S3). In addition to curing days as a variable, spreading behavior for the different aldehyde to amine ratios can be compared at a constant curing time (Fig. 3e shows 1 day curing as an example). The highest $\Delta L$ and $\Delta H$ are observed in the lowest mixing ratio (lower crosslinking) and reach the plateau region faster than for higher mixing ratios (higher crosslinking).

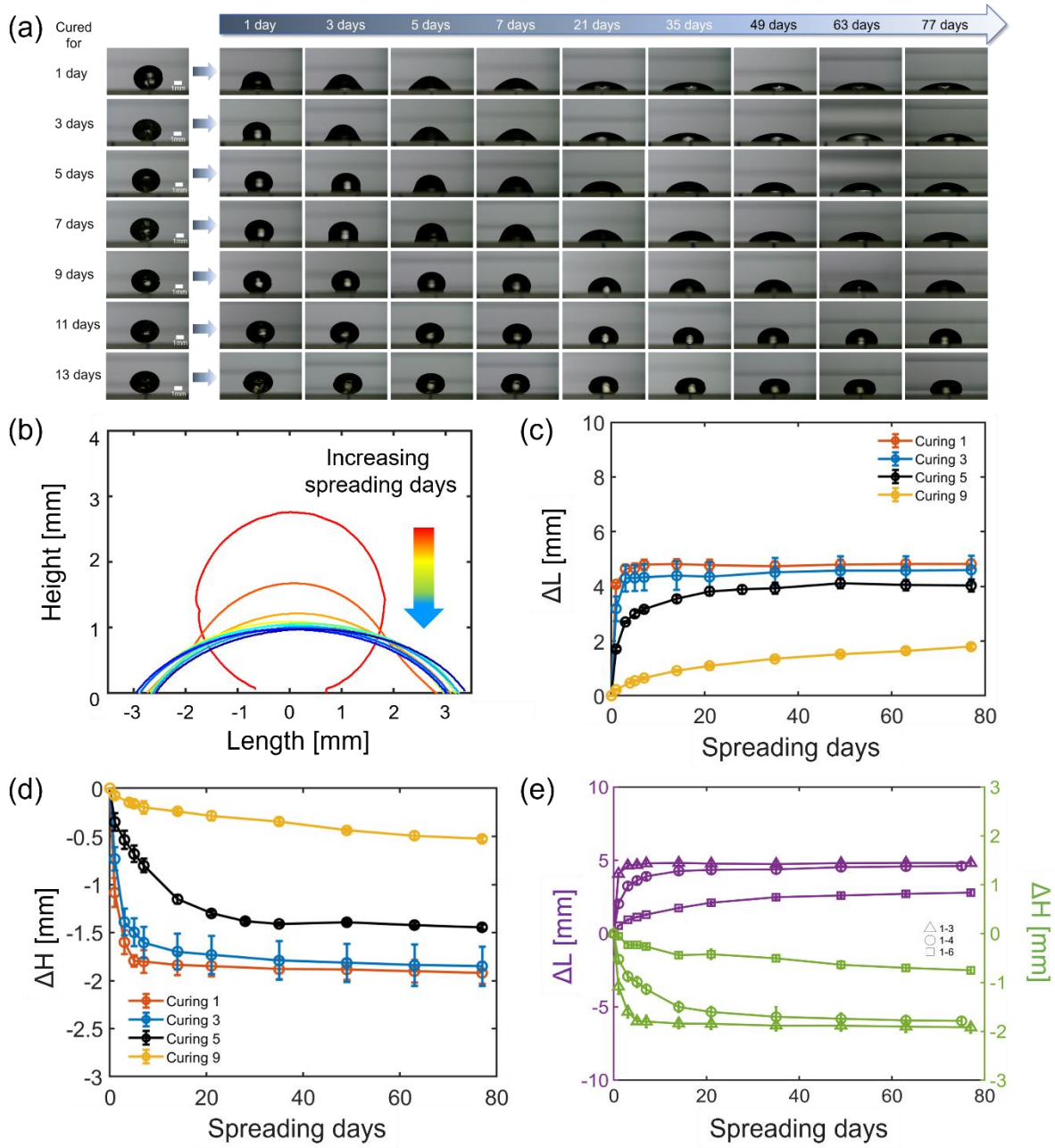


Figure 4. (a) Spreading of imPDMS of 1:3 ratio on fluorinated glass curing time, (b) Spreading profile, (c) length change ($\Delta L$), (d) length change ($\Delta H$) of 1:3 ratio, and (e) $\Delta L$ and $\Delta H$ for different mixing ratio at curing 1 day on fluorinated glass

*Spreading on fluorinated glass*. To investigate the spreading of dynamic networks in relation to surface energy, imPDMS drops are placed onto fluorinated glass substrates that have lower surface energy than unmodified glass[51]. The difference in surface energy is confirmed through a water drop contact angle measurement (Fig. S4). The qualitative results for the 1:3 mixing ratio are presented in Fig. 4, in a similar fashion to Fig. 3. For curing times up to 7 days, a bell shape is observed similar to that on glass substrates; however, the foot formation is less distinct since the driving force (surface energy) for spreading is lower on the fluorinated surface (Fig. 4a). Hence, the rate of change in spreading length ($\Delta L$) is slower compared to unmodified glass. Consequently, a drop-like spherical cap is maintained without the fried egg stage, even for imPDMS with low curing times. These findings illustrate that surface energy plays an important role in the spreading shape. It confirms that surface energy serves as the main driving force that controls the extent of spreading while the dynamic network rheology relates to the shape and rate of the spreading drops. The spreading profile on fluorinated glass exhibits smaller changes in contact length compared to glass (Fig. 4b). This is likely due to the lower driving force for spreading on fluorinated glass, allowing the drop to relax globally during the spreading process. $\Delta L$ and $\Delta H$ display exponential growth and decay, respectively, reaching a plateau similar to spreading on glass; however, the plateau is reached more quickly compared to unmodified glass (Figs. 4c and 4d vs. 3c and 3d). In addition to the curing days, the length and height changes with different mixing ratio of imPDMS similarly demonstrate slow spreading on fluorinated glass compared to unmodified glass for the same mixing ratios (Fig. 4e, SI Figs. S5 and S6).

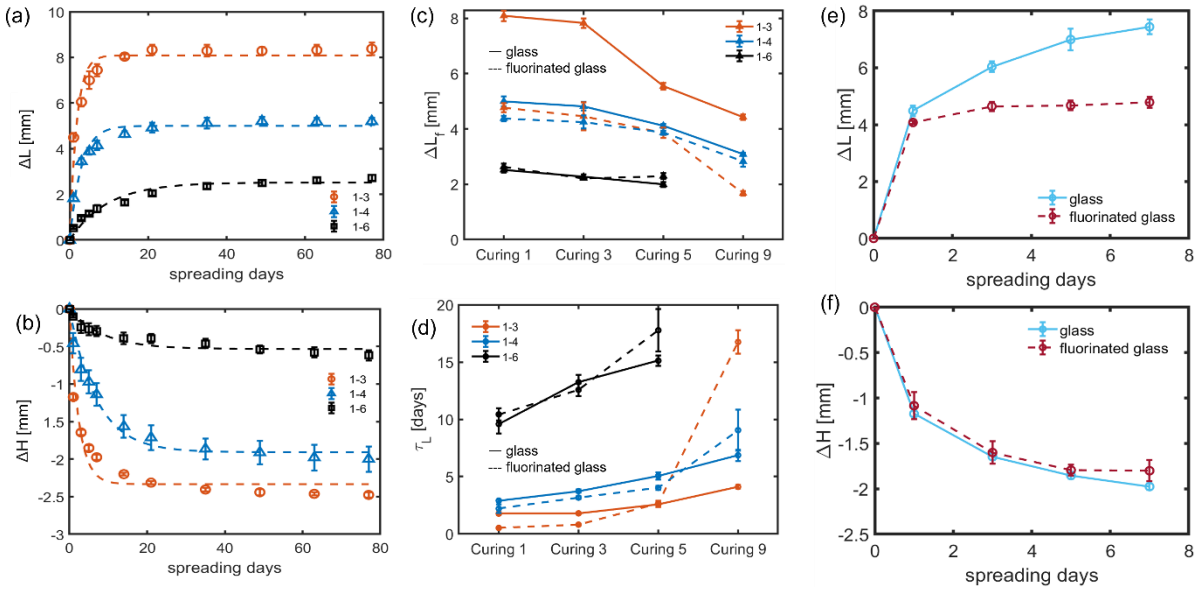


Figure 5. (a) Exponential fitting on (a) $\Delta L$ and (b) $\Delta H$ at curing 1 day on glass (c) a final spreading length change ($\Delta L_f$), (d) Characteristic time of $\Delta L$ ($\tau_L$), (e) $\Delta L$, and (f) ΔH of 1:3 ratio at curing 1 day for spreading 7 days.

*Description of spreading and variables*. The spreading process consists of two general regimes: a spreading phase and a plateau phase (Figs. 3 and 4). Based on our experimental results, the

first ~7 days are dominated by the spreading phase which then approaches the plateau towards an equilibrium length. To describe the rate and extent of spreading, we assume that the drop geometry grows (contact length) and decays (drop height) according to an exponential function. We can then write the change in length and height as $\Delta L(t) = \Delta L_f\left(1 - e^{-t/\tau_L}\right)$ and $\Delta H(t) = -\Delta H_f\left(1 - e^{-t/\tau_H}\right)$, respectively; $\tau_L$ and $\tau_H$ are characteristic times associated with the time it takes to approach the final change in length $\Delta L_f$ and height $\Delta H_f$. Our data are fit to these equations using a two-parameter fit to extract $\tau_L$ and $\Delta L_f$ as well as $\tau_H$ and $\Delta H_f$, enabling us to compare the extent of spreading as well as the rate of spreading, relative to the final geometry. The fits (dotted lines) are shown in Figs. 5a ($\Delta L$) and 5b ($\Delta H$) for the three mixing ratios at 1 day of curing, showing that the model is able to capture the trends in experimental data (see SI Figs. S7 and S8 for additional fits). Measured values for $\Delta L_f$ and $\Delta H_f$ after 77 days of spreading are consistent with the fit.

Let us first consider the spreading contact length on unmodified glass surfaces (Fig. 5c, solid lines). At a constant amount of curing, the 1:3 crosslinker ratio (orange solid lines) displays the largest $\Delta L_f$, which decreases when increasing the mixing ratio to 1:4 (blue solid lines) and 1:6 (black solid lines). At a constant mixing ratio, the amount of curing plays a significant role for the 1:3 mixing ratio, whereas curing days plays a small role in the 1:6 mixing ratio. For example, $\Delta L_f$ changes from ~8 mm to 5 mm for the 1:3 ratio but only ~2.5 mm to 2 mm for the 1:6 ratio for the 1 day and 9 day curing times. This clearly illustrates that the spreading is strongly governed by the degree of crosslinking. A similar trend is observed for $\Delta H_f$ (Fig. S9a), but with smaller changes.

Considering the two different surfaces, we find that $\Delta L_f$ and $\Delta H_f$ are higher on glass (Fig. 5c and Fig. S9a, solid lines) compared to fluorinated surfaces (Fig. 5c and Fig. S9a, dashed lines). This results from the higher surface energy of unmodified glass that drives spreading compared to fluorinated glass. The effect of surface energy is more dominant for lower mixing ratio materials (i.e. softer drops). For example, consider the 1 day curing samples; the 1:3 mixing ratio changes from $\Delta L_f$ ~8 mm to 5 mm when changing from glass to fluorinated glass, the 1:4 from ~5 mm to 4 mm, and the 1:6 remains nearly constant.

In addition to the extent of spreading, we also consider the rate of the spreading process through the fitted values of $\tau_L$ and $\tau_H$. Based on literature, one would anticipate that $\tau_L$ and $\tau_H$ increase with both increasing mixing ratio and increasing curing days, since both lead to higher modulus and longer relaxation times[52]. Consistent with this expectation, $\tau_L$ and $\tau_H$ increase with mixing ratio and curing time (Fig. 5d and Fig. S9b).

As can be seen in Fig. 5d, $\tau_L$ values for unmodified glass can be slightly higher than for fluorinated glass. This is because $\tau$ is associated with the final spreading geometry. imPDMS spreads to a larger extent on the unmodified glass (i.e. larger $\Delta L_f$, see Fig. 5c) compared to spreading on fluorinated glass (smaller $\Delta L_f$). Hence, the drops reach their final state faster on fluorinated surfaces, although the spreading speed itself is faster on glass surfaces from an

absolute sense (Fig. 5e). The change in height on the other hand does not significantly change with the underlying surface (Fig. 5f). This is consistent with the concept that lateral spreading is driven by surface energy while the drop height reduction is mainly governed by macroscopic relaxation.

## Conclusions

In this paper, we experimentally investigate the spreading of imPDMS, which is a silicone-based polymer network crosslinked with reversible imine bonds. Our results illustrate that it is important to consider the material composition (e.g. mixing ratio of components) and the processing conditions (e.g. curing time), which results in different viscoelastic properties. Although the mechanical properties play a dominating role in the spreading behavior, the surface energy of the underlying substrate must also be considered since it plays a role in the final contact length of the drop; the surface energy effects are particularly prominent for softer compositions. Future studies should consider the range of possible processing conditions, including temperature and humidity during spreading, as well as the material formulation, including the number of available amine groups and the polymer molecular weight.

## Methods

### Preparation of imPDMS drops

An imPDMS solution is prepared by mixing 6-7% aminopropylmethylsiloxane-dimethylsiloxane ($M_w$ = 4000-5000 g/mol, Gelest) with terephthalaldehyde (99%, Sigma-Aldrich) at molar ratios of 1:3, 1:4 and 1:6, which is also dissolved in tetrahydrofuran (Sigma-Aldrich) [23]. After mixing and degassing, 10 µl of solution mixture is dropped onto the end of a Teflon rod (D = 1/8 in, McMaster-Carr) and cured in an oven at 65°C for varying durations from 1 to 13 days. The shape of the imPDMS is nearly hemispherical as it sits on the cylindrical end of the Teflon rod. Two cured hemispheres are attached together to form imPDMS 'spheres' for the spreading experiments.

### Preparation of substrates

Glass substrates are prepared by washing under sonication with isopropanol for 5 min. Fluorinated glass is produced by subjecting these cleaned glass slides to a chemical vapor deposition using (1*H*,1*H*,2*H*,2*H*)-perfluorooctyl trichlorosilane (Sigma-Aldrich)[51] for 2 hours.

### Characterization

***Rheology.*** A rheometer (TA Instruments Discovery HR-2) equipped with 8-mm aluminum parallel plates is used to study rheological behavior of imPDMS. Samples are prepared by curing on a flat Teflon plate in an oven for 65°C, to mimic the sample preparation of imPDMS drops for spreading experiments, and then cut using an 8 mm diameter punch. Each sample is

tested over a frequency range from 10 Hz to $10^{-4}$ Hz at 0.5% strain. An amplitude sweep was conducted first to confirm this strain value was within the linear viscoelastic region.

***Image Analysis*.** Each spreading image is captured by a digital camera equipped with 0.5x zoom lens. The length, height, and shape are analyzed using MATLAB. Shape profiles of imPDMS are generated using MATLAB by stacking each captured spreading image. The outline of imPDMS is extracted from each image and assembled into a single coordinate. Length and height change during spreading are fit using MATLAB.

## Conflicts of interest

There are no conflicts of interest to declare.


## Acknowledgements

This work was supported by the US National Science Foundation (NSF) through CBET 2326933 and 2043732, and additionally by the National Research Foundation of Korea (NRF) funded by the Korea government (MSIT) (RS-2023-00277937 and RS-2023-00258475).

**References**


1. Li, L. Q.; Peng, X. T.; Zhu, D.; Zhang, J.; Xiao, P. Recent Progress in Polymers with Dynamic Covalent Bonds. *Macromol. Chem. Phys.* **2023,** *224* (20), 25.
2. Maeda, T.; Otsuka, H.; Takahara, A. Dynamic covalent polymers: Reorganizable polymers with dynamic covalent bonds. *Prog. Polym. Sci.* **2009,** *34* (7), 581-604.
3. Zheng, N.; Xu, Y.; Zhao, Q.; Xie, T. Dynamic Covalent Polymer Networks: A Molecular Platform for Designing Functions beyond Chemical Recycling and Self-Healing. *Chemical Reviews* **2021,** *121* (3), 1716-1745.
4. Huang, S.; Kong, X.; Xiong, Y. S.; Zhang, X. R.; Chen, H.; Jiang, W. Q.; Niu, Y. Z.; Xu, W. L.; Ren, C. G. An overview of dynamic covalent bonds in polymer material and their applications. *European Polymer Journal* **2020,** *141*, 18.
5. Jia, Y.; Qian, J.; Hao, S.; Zhang, S.; Wei, F.; Zheng, H.; Li, Y.; Song, J.; Zhao, Z. New Prospects Arising from Dynamically Crosslinked Polymers: Reprogramming Their Properties. **2024,** *36* (21), 2313164.
6. Winne, J. M.; Leibler, L.; Du Prez, F. E. Dynamic covalent chemistry in polymer networks: a mechanistic perspective. *Polymer Chemistry* **2019,** *10* (45), 6091-6108.
7. Hammer, L.; Van Zee, N. J.; Nicolay, R. Dually Crosslinked Polymer Networks Incorporating Dynamic Covalent Bonds. *Polymers* **2021,** *13* (3), 34.
8. Son, D. H.; Bae, H. E.; Bae, M. J.; Lee, S.-H.; Cheong, I. W.; Park, Y. I.; Jeong, J.-E.; Kim, J. C. Fast, Localized, and Low-Energy Consumption Self-Healing of Automotive Clearcoats Using a Photothermal Effect Triggered by NIR Radiation. *ACS Applied Polymer Materials* **2022,** *4* (5), 3802-3810.
9. Feng, H.; He, Y.; Ma, M.; Gao, S.; Zhao, S.; Shan, X.; Yang, H.; Cao, P.-F. J. A. A. M.; Interfaces. Hybrid Dynamic Covalent Network-Based Protecting Layer for Stable Li-Metal Batteries. **2024,** *16* (10), 12374-12384.
10. Wang, J. K.; Ma, L. W.; Huang, Y.; Ren, C. H.; Yang, H.; Wang, Y. J.; Liu, T.; Zhang, D. W. Photothermally activated self-healing protective coating based on the "close and seal" dual-action mechanisms. *Compos. Pt. B-Eng.* **2022,** *231*, 12.
11. Mashkoor, F.; Lee, S. J.; Yi, H.; Noh, S. M.; Jeong, C. Self-Healing Materials for Electronics Applications. **2022,** *23* (2), 622.
12. Wu, Y.; Jiang, W.; Zhao, T.; Wang, J.; Zhang, X.; Chen, D.; Ma, Y.; Yang, W. A facile strategy for fabricating self-healable, adhesive and highly sensitive flexible ionogel-based sensors. *Journal of Materials Chemistry C* **2022,** *10* (45), 17309-17320.
13. Hao, C.; Liu, T.; Zhang, S.; Brown, L.; Li, R.; Xin, J.; Zhong, T.; Jiang, L.; Zhang, J. J. C. A high-lignin-content, removable, and glycol-assisted repairable coating based on dynamic covalent bonds. **2019,** *12* (5), 1049-1058.
14. Nogusa, T.; Cooper, C. B.; Yu, Z.; Zheng, Y.; Shi, Y.; Bao, Z. J. M. Tunable, reusable, and recyclable perfluoropolyether periodic dynamic polymers with high underwater adhesion strength. **2023,** *6* (7), 2439-2453.
15. Chen, M.; Wu, Y.; Chen, B.; Tucker, A. M.; Jagota, A.; Yang, S. Fast, strong, and reversible adhesives with dynamic covalent bonds for potential use in wound dressing. **2022,** *119* (29), e2203074119.

16. Yang, Y.; Zhu, B. P.; Yin, D.; Wei, J. H.; Wang, Z. Y.; Xiong, R.; Shi, J.; Liu, Z. Y.; Lei, Q. Q. Flexible self-healing nanocomposites for recoverable motion sensor. *Nano Energy* **2015,** *17*, 1-9.
17. Bai, Y.; Jing, Z.; Zhang, B.; Pan, Y.; Wang, Q.; Duan, X. Recyclable Wearable Sensor Based on Tough, Self-Healing, Adhesive Polyurethane Elastomer for Human Motion Monitoring. *ACS Applied Polymer Materials* **2023,** *5* (10), 8720-8734.
18. Li, X.; Zhang, T.; Song, B.; Yang, K.; Hao, X.; Ma, J. A double-dynamic-bond crosslinked multifunctional conductive hydrogel with self-adhesive, remoldability, and rapid self-healing properties for wearable sensing. **2024,** *35* (1), e6267.
19. Zhang, Y.; Qi, Y.; Ulrich, S.; Barboiu, M.; Ramström, O. Dynamic covalent polymers for biomedical applications. *Materials Chemistry Frontiers* **2020,** *4* (2), 489-506.
20. McCarthy, K. A.; Kelly, M. A.; Li, K.; Cambray, S.; Hosseini, A. S.; van Opijnen, T.; Gao, J. Phage Display of Dynamic Covalent Binding Motifs Enables Facile Development of Targeted Antibiotics. *Journal of the American Chemical Society* **2018,** *140* (19), 6137-6145.
21. Chatir, E.; David, A. H. G.; Gapin, A.; Goujon, A. Dynamic Covalent Synthesis Applied to Optoelectronic and Energy Materials: Design, Applications and Limitations. **2024,** *27* (20), e202400211.
22. Wang, Y. M.; Zhang, Y.; Su, L.; Hu, S. K.; Xiang, P.; Zhao, X. Y.; Liu, L.; Zhang, L. Q.; Gao, Y. Y. Viscoelasticity and self-healing property of dynamic covalent polymers: A molecular dynamics simulation. *Polymer* **2024,** *295*, 10.
23. Wang, P.; Yang, L.; Dai, B.; Yang, Z. H.; Guo, S.; Gao, G.; Xu, L. G.; Sun, M. Q.; Yao, K. L.; Zhu, J. Q. A self-healing transparent polydimethylsiloxane elastomer based on imine bonds. *European Polymer Journal* **2020,** *123*.
24. Zechel, S.; Geitner, R.; Abend, M.; Siegmann, M.; Enke, M.; Kuhl, N.; Klein, M.; Vitz, J.; Gräfe, S.; Dietzek, B.; Schmitt, M.; Popp, J.; Schubert, U. S.; Hager, M. D. Intrinsic self-healing polymers with a high E-modulus based on dynamic reversible urea bonds. *NPG Asia Materials* **2017,** *9* (8), e420-e420.
25. Capets, J. A.; Yost, S. F.; Vogt, B. D.; Pester, C. W. Rapid Self-Healing of Robust Surface-Tethered Covalent Adaptable Coatings. *n/a* (n/a), 2406277.
26. Kashem, M. N. H.; Liu, X.; Ding, Z.; Li, W. Spin-spray-assisted layer-by-layer assembly of thick polymer films with self-healing, UV-protection, and anti-fog properties. **2023,** *61* (11), 1040-1051.
27. Fang, Z.; Shi, Y.; Mu, H.; Lu, R.; Wu, J.; Xie, T. 3D printing of dynamic covalent polymer network with on-demand geometric and mechanical reprogrammability. *Nature Communications* **2023,** *14* (1), 1313.
28. Bijalwan, V.; Rana, S.; Yun, G. J.; Singh, K. P.; Jamil, M.; Schlögl, S. 3D Printing of Covalent Adaptable Networks: Overview, Applications and Future Prospects. *Polym. Rev.* **2024,** *64* (1), 36-79.
29. Liu, Z.; Hong, P.; Huang, Z. Y.; Zhang, T.; Xu, R. J.; Chen, L. J.; Xiang, H. P.; Liu, X. X. Self-healing, reprocessing and 3D printing of transparent and hydrolysis-resistant silicone elastomers. *Chem. Eng. J.* **2020,** *387*, 13.

30. Yuan, T.; Zhang, L.; Li, T.; Tu, R.; Sodano, H. A. 3D Printing of a self-healing, high strength, and reprocessable thermoset. *Polymer Chemistry* **2020,** *11* (40), 6441-6452.
31. Mineo, A. M.; Buck, M. E.; Katsumata, R. Molecular design of polymer coatings capable of photo-triggered stress relaxation via dynamic covalent bond exchange. **2021,** *59* (22), 2719-2729.
32. Ma, J.; Porath, L. E.; Haque, M. F.; Sett, S.; Rabbi, K. F.; Nam, S.; Miljkovic, N.; Evans, C. M. Ultra-thin self-healing vitrimer coatings for durable hydrophobicity. *Nature Communications* **2021,** *12* (1), 5210.
33. Yuan, R.; Luo, C.; Yang, Y.; He, C.; Lu, Z.; Ge, L. Self-Healing, High Adherent, and Antioxidative LbL Multilayered Film for Enhanced Cell Adhesion. **2020,** *7* (11), 1901873.
34. Condò, I.; Giannitelli, S. M.; Lo Presti, D.; Cortese, B.; Ursini, O. Overview of Dynamic Bond Based Hydrogels for Reversible Adhesion Processes. **2024,** *10* (7), 442.
35. Darby, D. R.; Lai, E.; Holten-Andersen, N.; Pham, J. T. Interfacial Adhesion of Fully Transient, Mussel-Inspired Hydrogels with Different Network Crosslink Modalities. **2021,** *8* (14), 2100319.
36. Li, Z.; Zhou, F.; Li, Z.; Lin, S.; Chen, L.; Liu, L.; Chen, Y. Hydrogel Cross-Linked with Dynamic Covalent Bonding and Micellization for Promoting Burn Wound Healing. *ACS Applied Materials & Interfaces* **2018,** *10* (30), 25194-25202.
37. Zhang, Z.; Wang, X.; Wang, Y.; Hao, J. Rapid-Forming and Self-Healing Agarose-Based Hydrogels for Tissue Adhesives and Potential Wound Dressings. *Biomacromolecules* **2018,** *19* (3), 980-988.
38. Wang, S.; Teng, N.; Dai, J.; Liu, J.; Cao, L.; Zhao, W.; Liu, X. Taking advantages of intramolecular hydrogen bonding to prepare mechanically robust and catalyst-free vitrimer. *Polymer* **2020,** *210*, 123004.
39. Schonhorn, H.; Frisch, H. L.; Kwei, T. K. KINETICS OF WETTING OF SURFACES BY POLYMER MELTS. *J. Appl. Phys.* **1966,** *37* (13), 4967-+.
40. Kwei, T. K.; Schonhor.H; Frisch, H. L. KINETICS OF WETTING OF SURFACES BY POLYMER MELTS. *J. Colloid Interface Sci.* **1968,** *28* (3-4), 543-&.
41. Yin, T. P. J. T. J. o. P. C. Kinetics of spreading. **1969,** *73* (7), 2413-2417.
42. Rafaï, S.; Bonn, D.; Boudaoud, A. Spreading of non-Newtonian fluids on hydrophilic surfaces. *J. Fluid Mech.* **2004,** *513*, 77-85.
43. Gorin, B.; Di Mauro, G.; Bonn, D.; Kellay, H. Universal Aspects of Droplet Spreading Dynamics in Newtonian and Non-Newtonian Fluids. *Langmuir* **2022,** *38* (8), 2608-2613.
44. Tembely, M.; Vadillo, D.; Soucemarianadin, A.; Dolatabadi, A. Numerical Simulations of Polymer Solution Droplet Impact on Surfaces of Different Wettabilities. **2019,** *7* (11), 798.
45. Othman, A. M.; Poulos, A. S.; Torres, O.; Routh, A. F. Scalloped pattern deposition during the spreading and drying of polymer droplets. *Soft Matter* **2023,** *19* (44), 8483-8492.
46. Welygan, D. G.; Burns, C. M. PROFILES OF SPREADING SESSILE DROPS OF VISCOUS POLYMER MELTS. *J. Adhes.* **1982,** *14* (2), 129-136.

47. Son, Y.; Kim, C. Spreading of inkjet droplet of non-Newtonian fluid on solid surface with controlled contact angle at low Weber and Reynolds numbers. *J. Non-Newton. Fluid Mech.* **2009,** *162* (1-3), 78-87.
48. Belowich, M. E.; Stoddart, J. F. Dynamic imine chemistry. *Chemical Society Reviews* **2012,** *41* (6), 2003-2024.
49. Kulchat, S.; Chaur, M. N.; Lehn, J.-M. Kinetic Selectivity and Thermodynamic Features of Competitive Imine Formation in Dynamic Covalent Chemistry. **2017,** *23* (46), 11108-11118.
50. Chen, H.; Cui, C.; Ye, H.; Zou, H.; You, L. Enhancing hydrolytic stability of dynamic imine bonds and polymers in acidic media with internal protecting groups. *Chinese Chemical Letters* **2024,** *35* (5), 109145.
51. Badv, M.; Jaffer, I. H.; Weitz, J. I.; Didar, T. F. An omniphobic lubricant-infused coating produced by chemical vapor deposition of hydrophobic organosilanes attenuates clotting on catheter surfaces. *Scientific Reports* **2017,** *7* (1), 11639.
52. Chen, L.; Bonaccurso, E.; Shanahan, M. E. R. Inertial to Viscoelastic Transition in Early Drop Spreading on Soft Surfaces. *Langmuir* **2013,** *29* (6), 1893-1898.